Effects of mineral spatial distribution on reaction rates in porous media

L. Li,[1] C. A. Peters,[2] and M. A. Celia[2]

Received 3 January 2006; revised 21 July 2006; accepted 5 September 2006; published 27 January 2007.

[1] This study examined the effects of variations in mineral spatial distributions on reaction rates in porous media. Pore-scale network models were constructed to represent sandstones with anorthite and kaolinite present in various amounts and in different spatial patterns. Simulation conditions corresponded to geological sequestration of carbon dioxide. To examine scaling effects arising from pore-scale heterogeneities, reaction rates from network models were compared to rates from continuum models that use uniform concentrations. With small percentages of reactive minerals the scaling effects are large, and the effect of spatial distribution is significant. Scaling effects are largest when reactive minerals are closely clustered and oriented parallel to flow. Conversely, spatial distributions that enhance mass transport to and from reactive minerals, such as small mineral clusters or elongated clusters oriented transverse to flow, result in reaction rates that are well represented by the continuum model.

Citation: Li, L., C. A. Peters, and M. A. Celia (2007), Effects of mineral spatial distribution on reaction rates in porous media, *Water Resour. Res.*, *43*, W01419, doi:10.1029/2005WR004848.

1. Introduction

[2] Knowledge of reactive transport of chemical species in natural porous media is important for many problems [*Lichtner et al.*, 1996; *Steefel et al.*, 2005], including the geological sequestration of CO_2 [*Xu et al.*, 2003; *Knauss et al.*, 2005; *Spycher and Pruess*, 2005], remediation of contaminated groundwater [*Xu et al.*, 2000; *Mayer et al.*, 2002; *Steefel et al.*, 2003], nuclear waste disposal [*Tompson et al.*, 2000; *Van der Lee and De Windt*, 2001; *Metz et al.*, 2003; *De Windt et al.*, 2004; *Soler and Mader*, 2005], and alterations of geologic media as a result of water-rock interactions [*Lasaga and Rye*, 1993; *Steefel and Lasaga*, 1994; *Le Gallo et al.*, 1998; *Bolton et al.*, 1999]. Because of the large spatial and temporal scales involved in reactive transport processes and the difficulty of characterizing subsurface environments, the acquisition of such knowledge relies heavily on reactive transport simulations.

[3] Reactive transport models that involve mineral dissolution and precipitation reactions often use reaction kinetics measured in laboratory systems directly to calculate reaction rates in natural porous media. Because laboratory systems are often designed to be well mixed with no mass transport limitations, they can be very different from natural porous media where heterogeneities of various forms exist. Natural porous media are usually composed of multiple mineral phases, with some minerals more reactive than others. For example, many sandstones contain feldspars and clays, with their relative amounts varying over a wide range. Furthermore, these minerals can be distributed in different spatial patterns, depending on the composition of source rocks, depositional environments, and depositional and diagenetic processes [*Blatt*, 1992; *Carozzi*, 1993].

[4] The effect of physical heterogeneities on groundwater flow and solute transport in porous media has been studied for more than two decades [*Freeze*, 1975; *Dagan*, 1990; *Gelhar*, 1993; *Dagan*, 2004]. Recent studies on the effect of chemical heterogeneities of porous media on reactive solute transport have mainly focused on adsorption [*Tompson*, 1993; *Tompson and Jackson*, 1996; *Espinoza and Valocchi*, 1997, 1998; *Seeboonruang and Ginn*, 2006]. Very few studies have examined the effect of chemical heterogeneities on rates of geochemical reactions, such as mineral dissolution and precipitation reaction rates [*Meile and Tuncay*, 2006]. Our previous work has developed a novel application of pore-scale network modeling to investigate the effects of heterogeneities in pore structure and mineral distribution on geochemical reaction rates in porous media [*Li et al.*, 2006]. For anorthite and kaolinite in sandstone, we compared the scaling behavior of reaction kinetics under conditions relevant to geological sequestrations of CO_2. Simulation results showed that high acidity generates a large scaling effect, with order-of-magnitude variations in both aqueous concentrations and reaction rates within a spatial scale of less than one square centimeter. Using simpler models, based on a continuum approach that does not spatially resolve the pore space, the anorthite dissolution rate was overestimated by more than a factor of two and the kaolinite reaction direction cannot be correctly determined. In that work we limited the network modeling to a single configuration of mineral distribution, to focus on the cause for errors introduced when using simple upscaled models that do not account for pore-scale heterogeneity. This work extends that study by examining the effects of mineral spatial distributions on reaction rates and their scaling behavior in porous media.

[1] Earth Sciences Division, Lawrence Berkeley National Laboratory, Berkeley, California, USA.
[2] Department of Civil and Environmental Engineering, Princeton University, Princeton, New Jersey, USA.

0043-1397/07/2005WR004848$09.00

[5] As with our previous work, this work focuses on sandstones containing anorthite and kaolinite as reactive minerals. Anorthite was chosen because of its potential relevance to geological CO_2 sequestration [*Gunter et al.*, 2000; *Xu et al.*, 2004; *Gaus et al.*, 2005; *White et al.*, 2005] and because, as a Ca-containing feldspar, it is a primary sink for atmospheric CO_2 [*Walker et al.*, 1981; *Berner et al.*, 1983; *White and Brantley*, 1995]. The anorthite reaction is as follows:

$$CaAl_2Si_2O_8(s) + 8H^+ \rightleftharpoons Ca^{2+} + 2Al^{3+} + 2H_4SiO_4.$$

As anorthite commonly coexists with clay minerals, kaolinite is also modeled as a reactive mineral, with the following reaction:

$$Al_2Si_2O_5(OH)_4(s) + 6H^+ \rightleftharpoons 2Al^{3+} + 2H_4SiO_4 + H_2O.$$

Although quartz can be reactive [*Oelkers et al.*, 1996], under the same pH conditions its reaction rate is more than 6 orders of magnitude smaller than those of anorthite and kaolinite [*Kump et al.*, 2000]. As such, it is considered nonreactive (chemically inert) in this work. From a geochemical point of view, the reaction system is somewhat idealized. Anorthite is a plagioclase end-member and its reaction rate is relatively fast compared to other plagioclases that contain alkali constituents [*Blum and Stillings*, 1995]. Furthermore, as summarized by *Oelkers* [2005], there are numerous reactions that can occur when CO_2 is introduced into sedimentary rock formations. Our intent in focusing on this simple model system is to illustrate the scaling effects that can occur due to the nonlinear rate laws characteristic of mineral dissolution and precipitation.

[6] This work examines the effects of reactive cluster size and orientation on reaction rates. Although very little work has been done to characterize the sizes, orientations and spatial distributions of reactive mineral clusters, differences in these features can potentially generate conditions that alter reaction rate upscaling. Because the relative amount of reactive minerals varies over a wide range in natural porous media, we also examine the impact of the reactive mineral abundance. Overall, 33 networks were simulated, with four realizations in each case. All simulations were run under conditions relevant to geological CO_2 sequestration, because the elevated CO_2 concentrations generate acidic conditions important for scaling [*Li et al.*, 2006].

[7] This paper first briefly presents the pore-scale network modeling approach, which includes a discussion of the mineral distributions simulated. It then describes the method of calculating upscaled reaction rates, followed by simulation conditions. After that, simulation results are presented, followed by a section discussing the implications of the results.

2. Pore-Scale Network Modeling

[8] Network modeling provides a framework to describe dynamic processes in a random medium. A pore-scale network model discretizes the void space of a porous medium into a matrix of pores within a connected network, incorporating the properties of individual pores. With a detailed representation of the pore space, the processes of interest are simulated at the pore scale and can be summed up or averaged over the network to examine the system dynamics at the continuum scale. The advantages of pore-scale network modeling lie in its capability of linking processes and properties at the pore scale to a mechanistic understanding of process dynamics at the continuum scale. As such, it is an effective upscaling tool to bridge pore-scale processes to continuum-scale phenomena. This general approach has traditionally been used to investigate multiphase flow in porous media [*Celia et al.*, 1995; *Blunt*, 2001]. In recent years, these models have also been applied to examine chemical and biological processes, such as dissolution of organic pollutants [*Jia et al.*, 1999; *Dillard and Blunt*, 2000; *Zhou et al.*, 2000; *Held and Celia*, 2001; *Knutson et al.*, 2001], and biomass growth [*Suchomel et al.*, 1998; *Dupin et al.*, 2001]. This section describes the construction of the pore network, the spatial distributions of reactive minerals across the network, and the simulation of reactive transport processes at the pore scale. Details of the network construction and pore-scale reactive transport processes are documented by *Li et al.* [2006].

2.1. Network Construction

[9] Regular latticed 3-D network models were constructed to represent consolidated sandstones with different spatial distributions of reactive minerals. To focus on the effects of heterogeneities in chemical properties, all network models were assumed to have the same overall physical properties. The porosity of the network is approximately 0.14 and the permeability is 7.9×10^{-10} cm^2. The physical size of the network is $3.4 \times 3.4 \times 3.4$ mm^3, and the network contains 8000 pores ($20 \times 20 \times 20$ in each direction). This size is big enough to reach the size of a representative elementary volume (REV) so that the continuum-scale properties can be represented at the network scale [*Li et al.*, 2007]. The overall flow direction is the "z" direction. An effective resistance to flow and an effective cross-sectional area for diffusion is assigned to each pore-to-pore connection. There is no physical representation that distinguish pore bodies and pore throats, as is commonly done in this type of modeling. All void volume is modeled as being contained in pore bodies. Pore bodies do not have prescribed geometries; they are defined only in terms of surface area and volume. The steady state flow field was calculated before the simulation of reactive transport processes.

[10] Simulation of reactive transport processes at the pore scale requires several parameters for each pore i and for the connections between adjacent pores. These parameters were randomly assigned from statistical distributions which were based on literature data when available, with details discussed by *Li et al.* [2006]. Pore volume was assumed to have a lognormal distribution, with the mean for the log-transformed pore volume (mm^3) being -3.42, and standard deviation of 0.51 [*Lindquist et al.*, 2000]. This corresponds to an arithmetic mean of 6.6×10^{-4} mm^3. The surface area was assumed to have an exponential distribution, with mean 6.0 mm^2, corresponding to a medium surface area to volume ratio for consolidated sandstone, 1.3×10^4 cm^{-1} [*Sen et al.*, 1990; *Borgia et al.*, 1996; *Frosch et al.*, 2000]. The distribution of pore-to-pore hydraulic conductances followed a lognormal distribution, with the mean of the log-transformed values (cm^4 g Pa^{-1}) being -6.1 and variance 1.0. The hydraulic conductance between pores was corre-

lated to the sum of the logarithm of the adjacent pore volumes, with correlation coefficient 0.9. The cross-sectional area between two pores was calculated using Poiseuille's law and the value of conductance.

2.2. Spatial Distributions of Reactive Minerals

[11] In the network model, pores were classified as either nonreactive, with the solid being quartz, or as reactive, with anorthite and kaolinite each occupying half of the total surface area. The classification of pores as reactive or nonreactive allows study of the extremes in patterns of mineral distributions. In nonreactive pores, the surface areas of anorthite and kaolinite are zero. Given a specific total number of reactive pores, the total surface areas of anorthite and kaolinite for the network were fixed. To investigate the effects of different spatial distributions of reactive pores, the total number of reactive pores was first fixed at 12.5% of the total number of pores. For a given simulation, reactive pores were grouped in clusters of specified size, shape, and orientation. The notation XXYYZZ is used throughout to specify the size, shape, and orientation of reactive clusters by denoting the numbers of pores in the x, y, and z directions, respectively, with the total number of pores being XX $\times$ YY $\times$ ZZ. The location of each cluster was determined by randomly assigning pores in the network, with the restriction that the entire cluster is inside the network domain and clusters do not overlap. Because of the variability in pore surface area, for the 9 networks simulated with 12.5% reactive pores, the resulting total surface area of anorthite or kaolinite ranged from 29.7 to 30.8 cm^2, with mean 30.2 cm^2; this variation is small enough to consider the total surface area of reactive minerals as constant.

[12] To examine the effects of reactive cluster orientation, two network models were constructed for rectangular clusters of size $2 \times 2 \times 16$ (a total of 64 pores for each cluster), but of different orientation. There are a total of 16 clusters in the network, and the overall percentage of reactive pores is actually 12.8%. In the "transverse" case, the reactive pore clusters are oriented with the long dimension perpendicular to the main flow direction (i.e., XXYYZZ = 160202). In the "parallel" case, the long dimension is parallel to the main flow dimension (020216).

[13] To examine the effects of reactive cluster size for the case where reactive minerals occupy 12.5%, nine network models were constructed with reactive clusters of cubic shape, but of sizes ranging from 010101, 020202, ..., to 101010. The smallest cluster size is one pore (010101), and there are 1000 clusters randomly distributed across the network; the largest cluster size (101010) is that of a single cluster containing all reactive pores in the network (1000 pores). For the latter case, the cluster was not randomly positioned; it was positioned in the center of the network.

[14] The effects of the relative amount of reactive minerals were examined with the percentage of reactive minerals ranging from relatively small to abundant, with nominal values of 6.25%, 12.5%, 25%, and 50%. For each percentage, the cluster size was chosen and the clusters were distributed using the methods just described for the 12.5% case. For the larger percentages, such as 50%, many of the cluster sizes do not fit within the network. As such, there were fewer available cluster sizes to be examined in these cases.

2.3. Reactive Transport Processes at the Pore Scale

[15] In individual pores, the masses of chemical species in the aqueous phase change due to advection, diffusion, and reaction. The relevant reactions include instantaneous reactions and the dissolution and precipitation reactions of anorthite and kaolinite, which were modeled kinetically. The instantaneous reactions that were modeled include the water dissociation reaction, and the speciation reactions of carbon-bearing species, silica-bearing species, and aluminum-bearing species; these sum up to nine reactions in total. There are fourteen aqueous species involved: Ca^{2+}; H^+; OH^-; the carbon-bearing species $H_2CO_3^*$, HCO_3^-, CO_3^{2-}; the silica-bearing species H_4SiO_4, $H_3SiO_4^-$, $H_2SiO_4^{2-}$; and the aluminum-containing species Al^{3+}, $Al(OH)^{2+}$, $Al(OH)_2^+$, $Al(OH)_3$, $Al(OH)_4^-$. The aqueous concentrations of these species in an individual pore were assumed to be uniform, because the kinetic reactions are so slow that the relatively fast mass transport eliminates the concentration gradient within the aqueous phase [*Li et al.*, 2006].

[16] The mass balance equations, which were developed following Lichtner's systematic formulation [*Lichtner*, 1985, 1996], were written for five key components: Ca^{2+}, C_T, Si_T, Al_T, and H_T. C_T collectively represented all carbon-bearing species, Si_T represented the summation of all silica-bearing species, Al_T represented the summation of all aluminum-bearing species, and the total aqueous proton H_T was computed as $[H_T] = -[Al(OH)^{2+}] - 2[Al(OH)_2^+] - 3[Al(OH)_3] - 4[Al(OH)_4^-] + [H_4SiO_4] - [H_2SiO_4^-] + [H_2CO_3^*] - [CO_3^{2-}] + [H^+] - [OH^-]$. These five mass balance equations, together with the nine mass action laws corresponding to the nine instantaneous reactions, are sufficient to describe the mass change in the aqueous phase in an individual pore.

[17] The mass balance equation, which accounts for advection, diffusion between adjacent pores, and reaction in pore i, is as follows:

$$V_i \frac{d[\cdot]_i}{dt} = \sum_{\substack{j=1 \\ Q_{ij}>0}}^{nc} Q_{ij}[\cdot]_j + \sum_{\substack{j=1 \\ Q_{ij}<0}}^{nc} Q_{ij}[\cdot]_i + \sum_{j=1}^{nc} D^*_{ij,\cdot}\, a_{ij} \frac{\left([\cdot]_j - [\cdot]_i\right)}{l} + S_{i,\cdot}, \quad (1)$$

where $[\cdot]$ represents the concentration of one of the five key components; V_i is the volume of pore i; j is the index for a pore that is connected to pore i; nc is the total number of pores connected to pore i; Q_{ij} symbolizes the flow rate between pore i and j; $D^*_{ij,\cdot}$ is the effective diffusion coefficient; a_{ij} is the cross-sectional area between pore i and j; and $S_{i,\cdot}$ denotes the mass change rate due to kinetic reactions. Because the network was assumed to be regular latticed, the distance between the centroids of connected pores, l, is a constant. Details of calculating "effective" diffusion coefficients were described by *Li et al.* [2006]. By taking into account variability in flow velocity at the pore scale, the network model explicitly incorporates the effect of hydrodynamic dispersion at the continuum scale.

[18] The last term in equation (1), $S_{i,\cdot}$, represents the mass change rate due to anorthite and kaolinite dissolution and

precipitation reactions. As discussed by *Li et al.* [2006], we made the assumption that these kinetic reactions occur only in reactive pores, that is, precipitation is not allowed in pores in which there is no reactive mineral surface. This assumption is based on the fact that precipitation occurs in two sequential steps: nucleation and crystal growth. Since the nucleation step has to overcome a surface free energy barrier, it is often the rate-limiting step [*Steefel and Van Cappellen*, 1990; *Lasaga*, 1998; *Giammar et al.*, 2005]. In nonreactive pores, due to the lack of reactive mineral surface, nucleation is more difficult to initiate, and precipitation occurs at a much slower rate than in reactive pores. Besides the theoretical basis, simulations were carried out to compare the case where kaolinite precipitation is allowed to occur in nonreactive pores and the case where it is not. Simulation results show that unless the amount of the kaolinite surface area in nonreactive pores is comparable to that in reactive pores, the inclusion of precipitation in nonreactive pores does not make a significant difference. This indicates that ignoring precipitation of kaolinite in nonreactive pores is valid for the time frame we consider.

[19] The reaction term takes different forms for different components, depending on the reactions involved:

$$S_{i,\mathrm{Ca}^{2+}} = r_{A,i}\mathcal{A}_{A,i} \tag{2}$$

$$S_{i,\mathrm{C}_T} = 0 \tag{3}$$

$$S_{i,\mathrm{Si}_T} = 2r_{A,i}\mathcal{A}_{A,i} + 2r_{K,i}\mathcal{A}_{K,i} \tag{4}$$

$$S_{i,\mathrm{Al}_T} = 2r_{A,i}\mathcal{A}_{A,i} + 2r_{K,i}\mathcal{A}_{K,i} \tag{5}$$

$$S_{i,\mathrm{H}_T} = -6r_{A,i}\mathcal{A}_{A,i} - 4r_{K,i}\mathcal{A}_{K,i} \tag{6}$$

where $\mathcal{A}_{A,i}$ and $\mathcal{A}_{K,i}$ are the surface areas of anorthite and kaolinite in pore i, respectively. The two reaction rates, $r_{A,i}$ and $r_{K,i}$, are local rates of anorthite and kaolinite reactions in pore i (mol cm^{-2} s^{-1}) respectively, calculated using the local concentrations.

[20] For anorthite and kaolinite, their reaction rates are the summation of the rates of three parallel reactions catalyzed by H^+, H_2O and OH^-. The rationale behind the choices of kinetic parameters is detailed by *Li et al.* [2006], with values based on literature data [*Oelkers and Schott*, 1995; *Amrhein and Suarez*, 1988; *Helgeson et al.*, 1984; *Brady and Walther*, 1989; *Ganor et al.*, 1995; *Carroll and Walther*, 1990; *Nagy et al.*, 1991]. While mineral reaction rates can be affected by many factors, such as temperature, concentrations of catalytic or inhibition ions, etc. [*Lasaga*, 1998], this work focuses on the effect of pH conditions and the concentrations of ions directly involved in the mineral reactions. Neglect of catalytic or inhibitory effects beyond those of H^+ is increasingly justified in CO_2 mediated reactions due to growing evidence that the effect of CO_2 on silicate dissolution rates can be accurately predicted by only accounting for the change in pH [*Carroll and Knauss*, 2005; *Golubev et al.*, 2005; *Pokrovsky et al.*, 2005]. In pore i, the specific form of the anorthite reaction rate law follows the one discussed by *Li et al.* [2006]:

$$r_{A,i} = \left(k_{\mathrm{H}}\{\mathrm{H}^+\}_i^{1.5} + k_{\mathrm{H_2O}} + k_{\mathrm{OH}}\{\mathrm{OH}^-\}_i^{0.33}\right)\left(1 - \Omega_{A,i}\right), \tag{7}$$

and the expression of $\Omega_{A,i}$ is:

$$\Omega_{A,i} = \frac{\{\mathrm{Ca}^{2+}\}_i\{\mathrm{Al}^{3+}\}_i^2\{\mathrm{H_4SiO_4}\}_i^2}{\{\mathrm{H}^+\}_i^8 K_{\mathrm{eq},A}}. \tag{8}$$

The reaction rate constants at 25 degree C are: $k_{\mathrm{H}} = 10^{-7.32}$, $k_{\mathrm{H_2O}} = 10^{-15.6}$, and $k_{\mathrm{OH}} = 10^{-17.5}$ mol cm^{-2} s^{-1}.

[21] In equations (7) and (8), $\{\cdot\}_i$ indicates the activities of aqueous species in pore i (mol/L); and K_{eq} denotes the equilibrium constant. The equilibrium constants of the two kinetic reactions and the nine instantaneous reactions are given by *Li et al.* [2006]. Activity is the product of the activity coefficient and the aqueous concentration $[\cdot]$. The saturation ratio Ω_i is an indicator of how far away the reaction is from equilibrium.

[22] Similarly, for kaolinite,

$$r_{K,i} = \left(k_{\mathrm{H}}\{\mathrm{H}^+\}_i^{0.4} + k_{\mathrm{OH}}\{\mathrm{OH}^-\}_i^{0.3}\right)\left(1 - \Omega_{K,i}^{0.9}\right), \tag{9}$$

with the following expression for $\Omega_{K,i}$:

$$\Omega_{K,i} = \frac{\{\mathrm{Al}^{3+}\}_i^2\{\mathrm{H_4SiO_4}\}_i^2}{\{\mathrm{H}^+\}_i^6 K_{eq,K}}. \tag{10}$$

Values of k_{H} and k_{OH} at 25 degree C are $10^{-14.8}$ and $10^{-19.7}$, respectively. Of the two reactive minerals, anorthite has a relatively fast dissolution rate, and its reaction releases Ca^{2+}, Al^{3+}, and H_4SiO_4, which, in a system where anorthite and kaolinite coexist, often drives kaolinite precipitation to occur.

3. Continuum-Scale Reaction Rates

[23] In this section the methods to calculate continuum-scale reaction rates are briefly described. More details are given by *Li et al.* [2006].

3.1. Rates From the Network Model: R_N

[24] For a porous medium, based on mass balance principles, the "true" reaction rate at the continuum scale is the mass change rate due to reaction at every reactive surface. As such, for anorthite, the continuum-scale reaction rate computed from the network model simulation is as follows:

$$R_{N,A} = \frac{\sum_{i=1}^{n}\mathcal{A}_{A,i}r_{A,i}}{\sum_{i=1}^{n}\mathcal{A}_{A,i}}, \tag{11}$$

where n is the total number of pores. An analogous equation follows for the calculation of the continuum-scale rate for kaolinite ($R_{N,K}$). These continuum-scale rates depend on local reaction rates ($r_{A,i}$ and $r_{K,i}$, respectively), and the presence of reactive minerals. Because reactions occur only in reactive pores, the continuum-scale reaction rates depend only on the concentrations in reactive pores, and are

insensitive to variations of concentrations in nonreactive pores.

3.2. Rates From the Continuum Model: R_C

[25] The continuum model is the fundamental building block of the continuum approach used in reactive transport modeling [*Lichtner*, 1996]. This model differs from the network model in that it ignores pore-scale heterogeneities, uses spatially averaged values to represent system properties, and utilizes uniform concentrations in laboratory-measured reaction rate laws to calculate the continuum-scale reaction rates. To compare the continuum-scale rates from the network and those from the continuum model, the continuum model was constrained to have the same hydrodynamic properties, total amounts of reactive minerals, and initial and boundary conditions as the network model.

[26] The reactions and species involved are the same as in the network model, and the mass balance equations follow the same systematic formulation for the five key components: Ca^{2+}, C_T, Si_T, Al_T, and H_T. For each key component, the form of the mass balance equation is as follows:

$$V_T \frac{d[\cdot]}{dt} = Q_T[\cdot]_{in} - Q_T[\cdot]_C + S_{C,\cdot}, \tag{12}$$

where V_T is the total pore volume across the network, $[\cdot]_{in}$ corresponds to the concentration at the inflow boundary, and $[\cdot]_C$ represents the uniform concentration in the continuum model. On the right side of the equation, the first two terms account for the mass changes due to advection, and the third term, $S_{C,\cdot}$, represents the mass change due to reaction. At the continuum scale, there is no diffusion term. The parameters used in the above equation represent spatially averaged properties of the porous media at the continuum scale.

[27] For each component, the rate term $S_{C,\cdot}$ takes the same form as those for the rate term in each pore (Equation 2 to 6), except that $r_{A,i}$ and $r_{K,i}$ are replaced by $R_{C,A}$ and $R_{C,K}$, respectively, and $\mathcal{A}_{A,i}$ and $\mathcal{A}_{K,i}$ are replaced by the total surface areas $\mathcal{A}_{A,T}$ and $\mathcal{A}_{K,T}$, respectively. For example, for Ca^{2+}, the reaction rate term takes the following form:

$$S_{C,Ca^{2+}} = R_{C,A}\mathcal{A}_{A,T}, \tag{13}$$

where $R_{C,A}$ is the reaction rate of anorthite. The reaction rates from the continuum model, $R_{C,A}$ and $R_{C,K}$, are calculated using the uniform concentrations in the reaction rate laws. For anorthite,

$$R_{C,A} = \left(k_H\{H^+\}_C^{1.5} + k_{H_2O} + k_{OH}\{OH^-\}_C^{0.33}\right)\left(1 - \Omega_{C,A}\right), \tag{14}$$

where $\Omega_{C,A}$ is the saturation ratio of anorthite reaction calculated using the uniform concentrations in reaction rate laws.

[28] The rate expression is similar for kaolinite, following the reaction rate law shown in Equations 9 and 10.

3.3. Comparison Between Continuum-Scale Reaction Rates

[29] Values of R_N are taken to represent the "true" reaction rates, because they incorporate the pore-scale heterogeneities, and are consistent with the mass balance of the network. We define the ratio:

$$\eta \equiv \frac{R_C}{R_N}, \tag{15}$$

as a measure of the effects of pore-scale heterogeneities and the scaling effect. If η is significantly different from unity, the effects of pore-scale heterogeneities are significant, and the use of uniform concentrations in laboratory-measured rate laws introduces large errors. Otherwise, the effects of pore-scale heterogeneities can be ignored, laboratory-measured rate laws can be used directly at the continuum scale, and the continuum model accurately simulates the reactive transport processes.

4. Simulation Conditions and Numerical Computation

[30] The simulations were run under conditions relevant to CO_2 sequestration, at a temperature of 323 K, a pressure of 10^7 Pa, and high salinity (with total dissolved salinity being 0.45 mol/L). All parameters involved in the simulation of reactive transport processes, such as reaction rate constants, equilibrium constants, and diffusion coefficients, were adjusted to such conditions, as documented by *Li et al.* [2006]. Because of the high salinity of brine, the activity coefficients were considered constant both in time and space, and were calculated using the Davies equation [*Morel and Hering*, 1993].

[31] Initially the brine was assumed to have a uniform concentration throughout the network and to be in equilibrium with quartz and kaolinite, at pH 7.5, which fixed the initial values of Si_T, Al_T, and H_T. The initial Ca^{2+} concentration (7.9×10^{-6} mol/L) was calculated from the electronic neutrality condition, given concentrations of Si_T, Al_T, and H_T. Initially the concentrations of the carbon-bearing species are zero, corresponding to formations with negligible concentrations of naturally occurring carbon dioxide. The brine at the inflowing boundary is assumed to have the same $[Ca^{2+}]$ as in the initial aqueous phase within the network, and its C_T concentration was calculated based on equilibrium with carbon dioxide at a pressure of 10^7 Pa, which is within the expected range of injection pressures for CO_2. The solubility of CO_2 was calculated using the semiempirical relationship from *Duan and Sun* [2003]. Because of the large amount of CO_2 dissolved in the boundary brine, the boundary pH is 2.9. The porous medium is assumed to be close to a CO_2 injection well, and we chose a flow velocity of 4.6×10^{-3} cm/s, which is consistent with such a condition of proximity to an injection well [*Knapp*, 1989; *Harter*, 2003].

[32] To keep the porosity change relatively small so that the permeability change is within 5%, simulations were run within a limited time frame. As such, the porosity and permeability of the porous medium were considered constant during the simulation process. For the same reason the values of pore volumes and the mineral surface area were also considered constant during the simulation. Therefore the present modeling work is based on constant temperature, ionic strength, and surface area of reactive minerals. This allowed the system to eventually reach steady state,

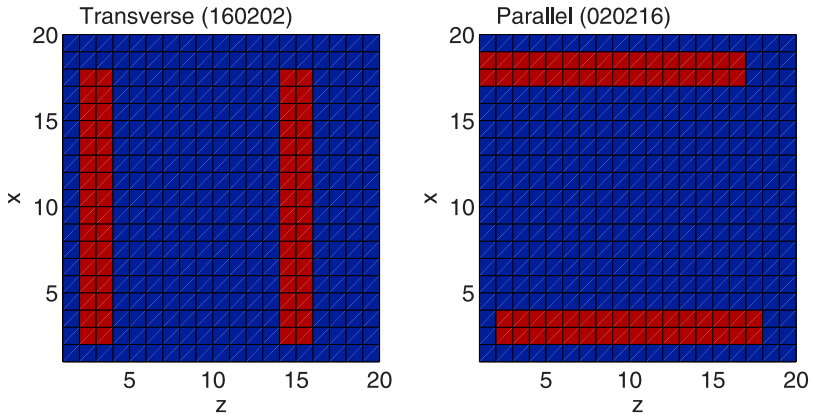

Figure 1. Placement of reactive clusters for a slice in the middle of the network (y = 10) for the transverse (160202) and parallel (020216) cases where nominally 12.5% of the pores contain reactive minerals.

with constant concentrations of the aqueous species and the reaction rates in terms of time.

[33] The time it takes to reach a steady state generally depends on the flow velocities used. In this work, it takes about four to five hundred seconds.

[34] The numerical approach used is identical to that used in our previous work [*Li et al.*, 2006].

5. Results

[35] The simulation results are first presented for the case in which nominally 12.5% of the pores are reactive. The effects of reactive cluster orientation and size on pore-scale concentrations and reaction rates, and on the continuum-scale reaction rates are examined. Results on the impact of the relative amount of reactive minerals on continuum-scale behavior follow.

5.1. Effects of Reactive Cluster Orientation

[36] In this section we compare the simulation results for two different spatial orientations of reactive minerals: transverse (160202) and parallel (020216), with nominally 12.5% of the pores containing reactive minerals and reactive cluster size of 64 pores. Figure 1 shows the placement of reactive pores in the middle slice of the network (y = 10) for these two cases.

[37] The steady state concentration fields of log [Ca^{2+}] and pH for the transverse and parallel cases are shown in Figure 2 for the middle slice of the network (y = 10). The highly acidic aqueous phase flows into the network from the left boundary. As this water enters reactive pores, anorthite dissolves and releases Ca^{2+}, which leads to an increase in pH. As such, the concentrations of Ca^{2+} and the pH in reactive pores are generally higher than those in nonreactive pores. Nonreactive pores may also have elevated Ca^{2+} concentrations and pH if they are close to or downstream from reactive pores.

[38] Although for both cases [Ca^{2+}] and pH are locally high in reactive pores, the spatial patterns of concentration distributions are quite different. For the transverse case, the concentrations are more evenly distributed, and concentrations in nonreactive pores are very much affected by concentrations in reactive pores. For the parallel case, concentrations in most of the nonreactive pores are not significantly influenced by concentrations in reactive pores and remain similar to those of the boundary aqueous phase. As a consequence, we see a clear distinction between concentrations in reactive and nonreactive pores.

[39] As mentioned in section 3.1, it is the concentrations in the reactive pores that ultimately determine the net reaction rate for the network. The distributions of concentrations in reactive pores are shown in Figure 3. Compared to the transverse case, the parallel case has a larger percentage of pores with high [Ca^{2+}] and high pH. Also shown in Figure 3 are values of the steady state concentrations from the continuum model simulations. The uniform concentrations from the continuum model are closer to the modes of the concentration distributions in the transverse case than in the parallel case, indicating that they represent the pore-scale concentrations better for the transverse case.

[40] The rate distributions of anorthite and kaolinite reactions in reactive pores are shown in Figure 4. Also shown in Figure 4 are the continuum-scale rates from the network model (the dotted lines), and the continuum-scale rates from the continuum model (the dot-dashed lines). Anorthite dissolves in all reactive pores, with the rates spanning almost an order of magnitude. Compared to the transverse case, the shape of the rate distribution is slightly more skewed in the parallel case, with a larger percentage of pores having smaller anorthite dissolution rates. This is because anorthite dissolution is slower under less acidic conditions, and in the parallel case, there is a larger percentage of pores having higher pH(less acidic conditions), as indicated in Figure 3. As a consequence, the continuum-scale anorthite dissolution rate from the network model is smaller in the parallel case than that in the transverse case.

[41] Kaolinite precipitates in most of the reactive pores, but it dissolves in some of the reactive pores. The rates span several orders of magnitude, with a larger percentage of reactive pores having larger kaolinite precipitation rates in the parallel case, because kaolinite precipitates faster in less acidic conditions. As a consequence, the continuum-scale kaolinite precipitation rate from the network model is larger in the parallel case than in the transverse case.

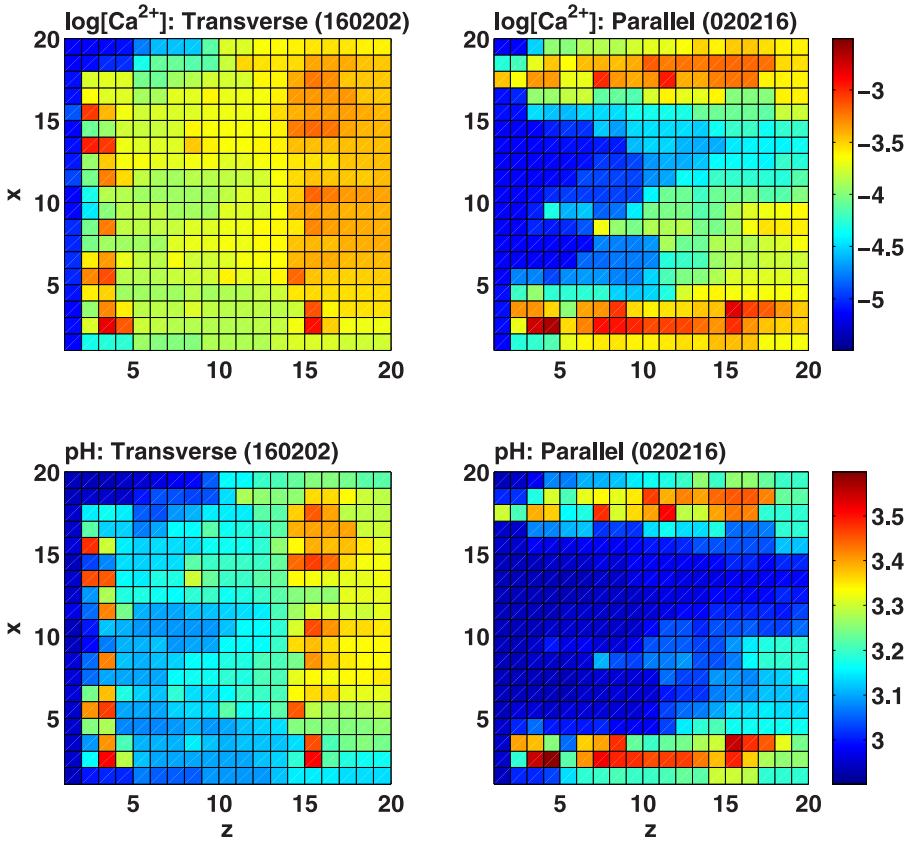

Figure 2. Steady state concentration fields for transverse (160202) and parallel (020216) cases for the middle slice of the network (y = 10).

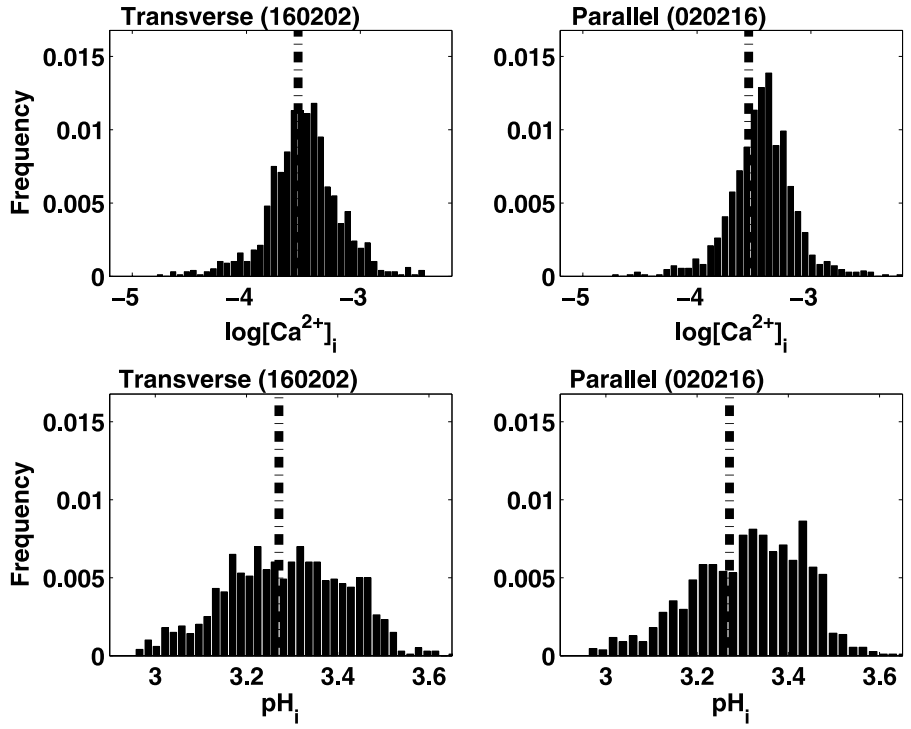

Figure 3. Distributions of steady state concentrations in reactive pores for transverse (160202) and parallel (020216) clusters. The values of the steady state concentrations from the continuum model simulations are shown in dot-dashed lines.

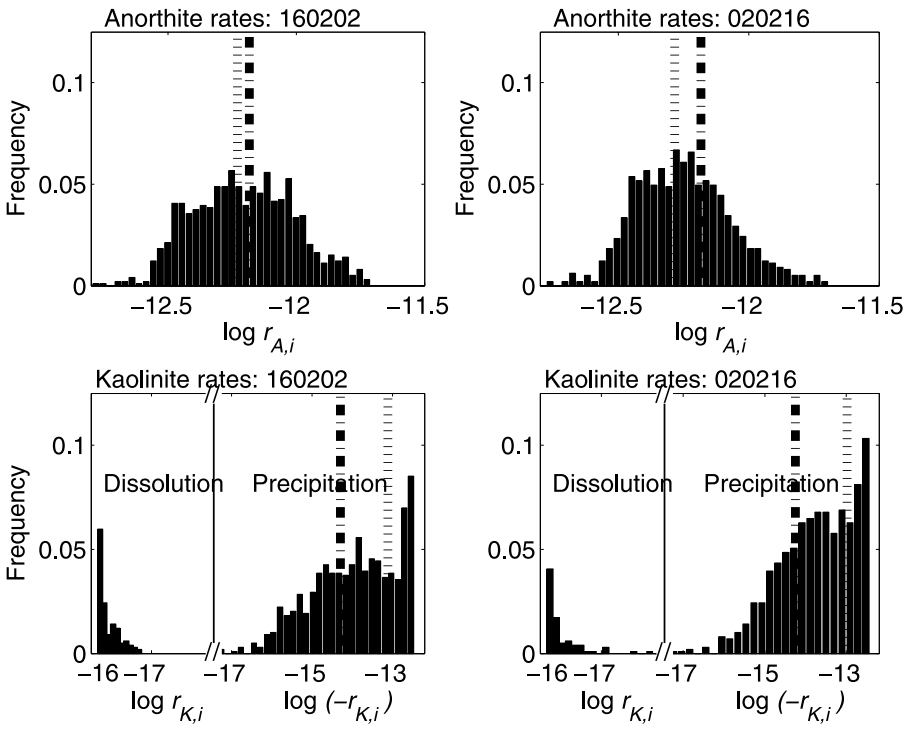

Figure 4. Distributions of steady state reaction rates in reactive pores for transverse (160202) and parallel (020216) reactive clusters. The dotted lines are the continuum-scale rates from the network model, and the dot-dashed lines are rates from the continuum model.

[42] Because the continuum model does not spatially resolve concentrations below the scale of the entire network, it predicts the same concentrations and continuum-scale reaction rates for the two spatial orientations of reactive clusters. For both orientations, the continuum model slightly overestimates the anorthite dissolution rates, and significantly underestimates the kaolinite precipitation rates. The degrees of overestimation and underestimation are larger in the parallel case than in the transverse case, as indicated by the η values in Table 1.

5.2. Effects of Reactive Cluster Size

[43] To illustrate the effects of reactive cluster size, we start with an analysis of the concentration fields, concentration distributions, and reaction rates for the cases with the smallest cluster (010101, size of one pore), with medium clusters (040404, size of 64 pores), and with the largest cluster (101010, 1000 pores). With nominally 12.5% of pores containing reactive minerals, the numbers of clusters in the network for these three cases are 1000, 16, and 1, respectively. The spatial patterns of reactive clusters in the middle slice of the network ($y = 10$) for these three cases are shown in Figure 5. This section concludes with the simulation results for all nine network models for reactive clusters of cubic sizes with 12.5% reactive pores.

Table 1. Steady State Values of η and R_N for Different Spatial Distributions of Reactive Mineral Clusters for the Percentage of Reactive Minerals Being Nominally 12.5%[a]

Spatial Distributions	η_A	$R_{N,A}$	η_K	$R_{N,K}$
Transverse (160202)	1.1	5.9×10^{-13}	0.066	-6.2×10^{-14}
Parallel (020216)	1.3	5.1×10^{-13}	0.050	-8.2×10^{-14}
Small (010101)	1.1	6.1×10^{-13}	0.074	-5.5×10^{-14}
Medium (040404)	1.2	5.4×10^{-13}	0.058	-7.1×10^{-14}
Large (101010)	1.4	4.6×10^{-13}	0.035	-1.2×10^{-13}

[a]Units of all reaction rates are in mol cm^{-2} s^{-1}. For all cases, $R_{C,A} = 6.5 \times 10^{-13}$, and $R_{C,K} = -4.1 \times 10^{-15}$ mol cm^{-2} s^{-1}.

5.2.1. Concentration Distributions

[44] The characteristics of the steady state concentration fields vary significantly with the size of reactive clusters, as shown in Figure 6 for the middle slice of the network ($y = 10$). In the case of the smallest cluster (010101), pores with locally high [Ca^{2+}] and pH are distributed over the entire network, and there is no clear distinction between reactive and nonreactive pores. The concentrations in nonreactive pores are largely affected by concentrations in reactive pores. In contrast, for the case of the largest cluster (101010), the concentration field clearly shows two distinct regions: the high [Ca^{2+}] and high pH region corresponding to concentrations in reactive pores, and the low [Ca^{2+}] and low pH region corresponding to concentrations in nonreactive pores. In most of the nonreactive pores, concentrations remain largely the same as boundary concentrations. There are more pores that have high concentrations of Ca^{2+} and high pH than in the case of smallest cluster. For medium-sized reactive clusters (040404), the result falls in between these two extremes. There are regions with high [Ca^{2+}] and high pH, but the distinction between the reactive and nonreactive regions is not very sharp.

[45] The distributions of log [Ca^{2+}] and pH in all pores for different sizes of reactive clusters are shown in Figure 7. Consistent with the characteristics of the concentration fields for a single layer, the distributions of pore-scale concentrations differ significantly. In the case of the largest cluster (101010), the distributions are quite bimodal, which

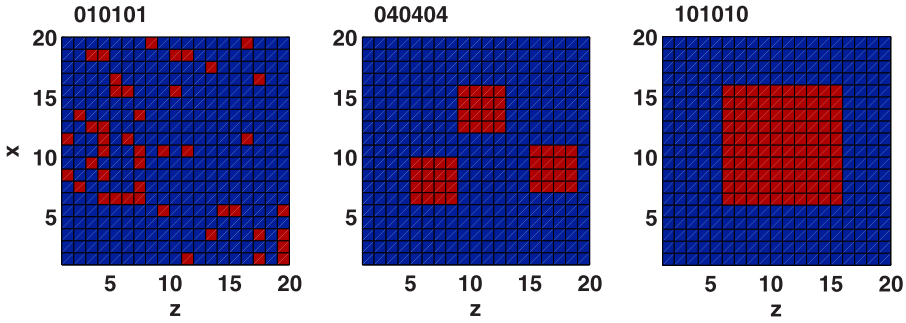

Figure 5. Spatial patterns of reactive minerals (red) for the middle slice of the network (y = 10), with different sizes of reactive clusters: smallest (010101), medium (040404), and largest (101010). In all cases, 12.5% of the pores in the network contain reactive minerals.

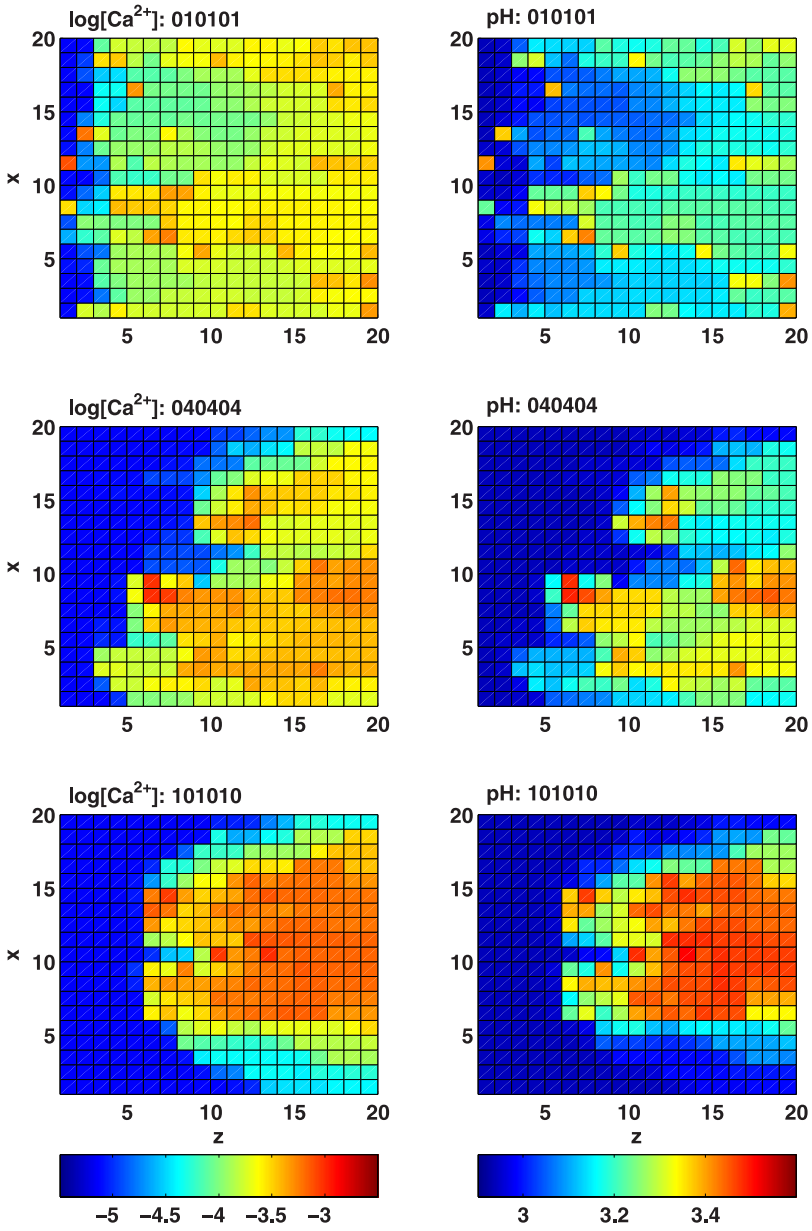

Figure 6. Steady state concentration fields of log[Ca^{2+}] and pH for the middle slice of the network (y = 10) for reactive clusters of size 010101, 040404, and 101010.

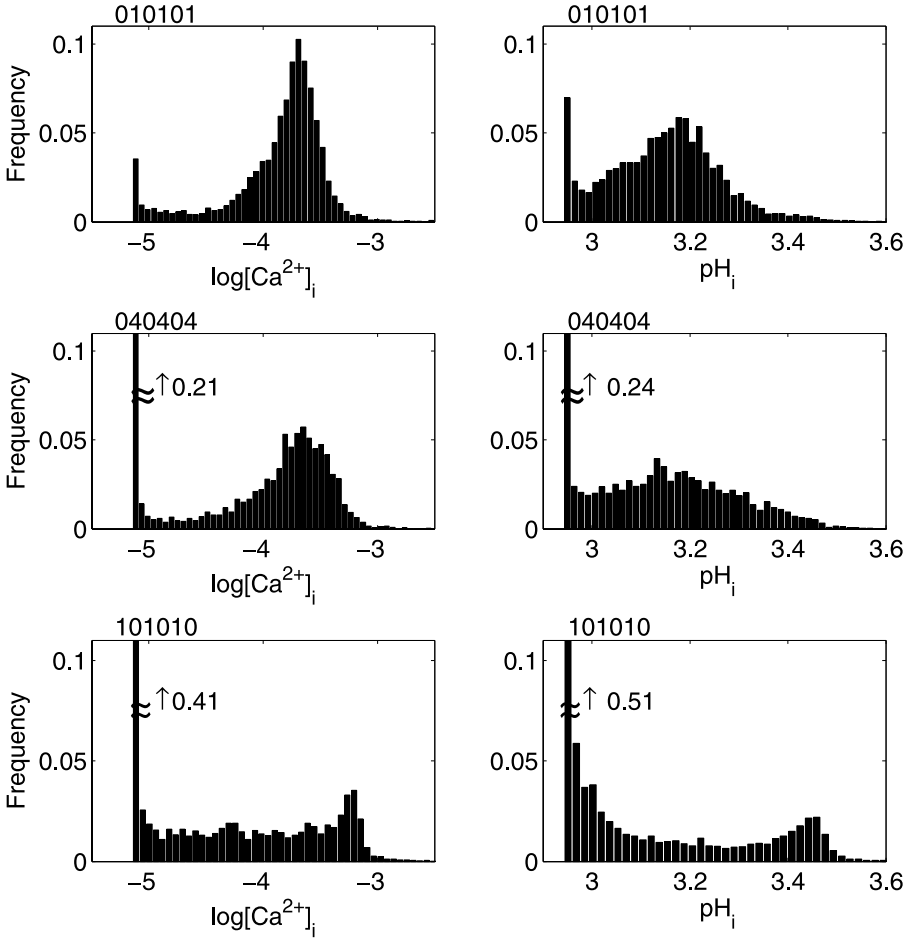

Figure 7. Distributions of steady state concentrations in all pores for different sizes of reactive clusters: smallest (010101), medium (040404), and largest (101010).

is consistent with the concentration fields showing two distinctive regions. One mode of the distribution is at log $[Ca^{2+}] = -5.1$ and pH = 2.9, showing that more than 40% of the pores have concentrations of the boundary condition. The other mode is at the high end of the concentration range, corresponding to log $[Ca^{2+}] = -3.2$ and pH = 3.5. For the case of the smallest cluster (010101), the percentage of pores having the boundary concentrations is less than 10%, and the concentrations in most of the pores fall in the middle of the concentration range (mode of log $[Ca^{2+}] = -3.7$ and pH = 3.2). The results for the medium-sized reactive clusters (040404) are between these two extremes. With increasing cluster size, the percentage of pores having small and large concentrations increases, leaving smaller numbers of pores with medium concentrations, indicating a sharper distinction between concentrations in reactive and nonreactive pores.

[46] The effects of reactive cluster size on concentration distributions in only the reactive pores are shown in Figure 8. For comparison, the uniform concentrations from the continuum model are also shown in dot-dashed lines. These values, log$[Ca^{2+}] = -3.55$ and pH = 3.29, are the same for all three cases. With the smallest cluster (010101), the concentration distributions are quite symmetric, with the mode of the distribution coinciding with the uniform concentration from the continuum model. With increasing cluster size, the distributions become skewed, with increasing percentage of pores having high concentrations of Ca^{2+} and high pH. For the intermediate case (040404), 50% of the reactive pores have pH values larger than 3.29, and for the largest case (101010), 85% of the reactive pores have pH values larger than 3.29.

5.2.2. Pore-Scale and Continuum-Scale Reaction Rates

[47] Because of the dependence of reaction rates on aqueous concentrations, the pore-scale concentration heterogeneities lead to spatial variations in pore-scale reaction rates. Figure 9 shows the distributions of anorthite and kaolinite reaction rates at steady state. Dissolution and precipitation occurs only in reactive pores, so the distributions actually show values only for these pores, but the frequencies have been normalized to the total number of pores in the network. Also shown in Figure 9 are the continuum-scale rates from the network model R_N (dotted lines) and from the continuum model R_C (dot-dashed lines).

[48] Anorthite dissolution remains far from equilibrium in all reactive pores, and the rate is largely determined by concentrations of hydrogen ions. As such, spatial variations in anorthite dissolution rates are largely determined by spatial variations in pH in reactive pores (Figure 8), and the distributions of log $r_{A,i}$ have a shape similar to that of the negative pH distributions in reactive pores. For the case of

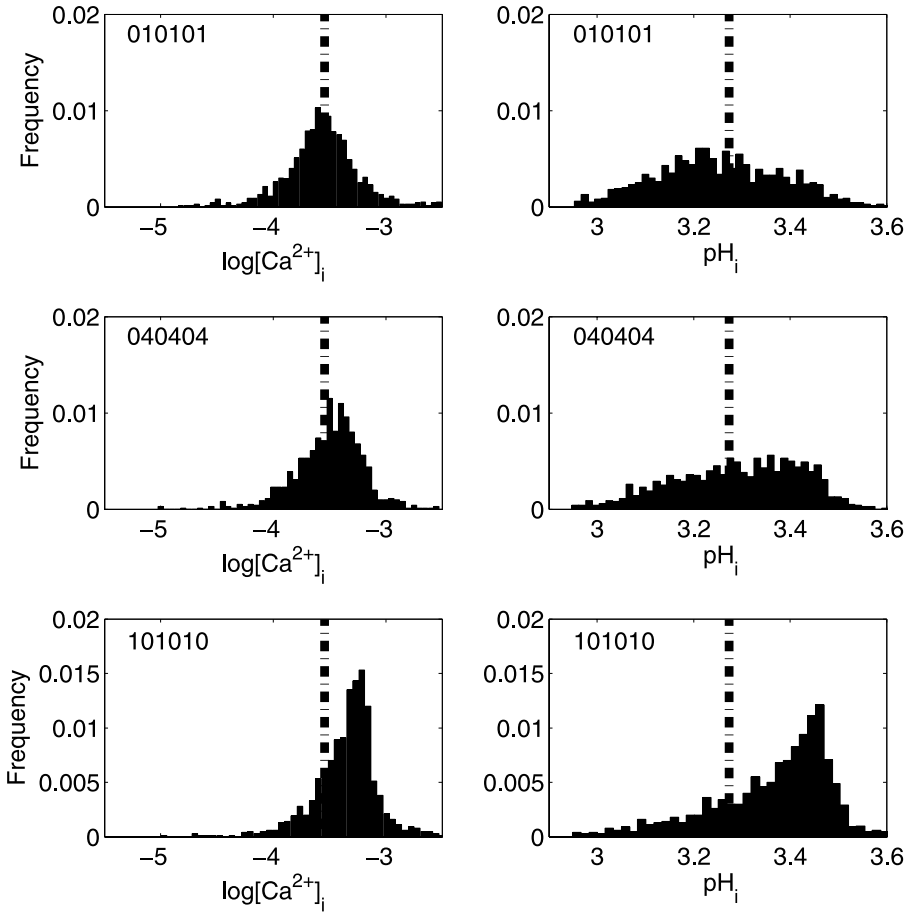

Figure 8. Distributions of steady state distributions of log[Ca^{2+}] and pH in reactive pores for reactive clusters of size 010101, 040404, and 101010. The dot-dashed lines are the uniform concentrations from the continuum model.

the smallest cluster (010101), the distribution is relatively symmetric. With increasing reactive cluster size, the distributions are more skewed, with a larger percentage of pores having small anorthite dissolution rates.

[49] The resulting continuum-scale rates from the network model decrease with increasing cluster size. The continuum model does not capture these effects and therefore predicts the same rates for these different cases. For the case of the smallest cluster (010101), the rate from the continuum model is almost equal to the rate predicted from the network model. With increasing cluster size, the continuum model increasingly overestimates continuum-scale anorthite dissolution rates, as indicated by an increasing difference between R_C and R_N.

[50] For kaolinite, precipitation occurs in most pores while dissolution occurs in others. With increasing size of reactive clusters, dissolution occurs in a smaller percentage of pores, and precipitation occurs at substantially larger rates in a larger percentage of pores. As a result, the continuum-scale kaolinite precipitation rates computed from the network model increase with reactive cluster size. The continuum model significantly underestimates the kaolinite precipitation rates in all cases, and the degree of underestimation increases with increasing cluster size. The differences between the continuum-scale rates from the continuum model and the network model are indicated by the η values in Table 1.

5.2.3. Comparison of Continuum-Scale Rates

[51] To illustrate the effects of cluster size on the reaction rates for the entire series of nine cluster sizes, Figure 10 shows the steady state continuum-scale rates of anorthite dissolution and kaolinite precipitation as a function of cluster size. Cluster size is quantified by length in pores (which is the same in each of the three dimensions because of the cubic shape). For comparison, the rates from the continuum model are also shown in dot-dashed lines. With increasing size of reactive clusters, anorthite dissolution rates decrease, while kaolinite precipitation rates increase. For anorthite dissolution, the rate with the smallest cluster (010101) is approximately 1.3 times the rate with the largest cluster size (101010); for kaolinite precipitation, the rate for the smallest cluster size (010101) is about one half times the rate with the largest cluster size (101010). The continuum model overestimates anorthite dissolution rate, and underestimates kaolinite precipitation rate, with the error increasing with the cluster size. For the largest cluster size, the estimate by the continuum model of the kaolinite precipitation rate is approximately two orders of magnitude smaller.

5.3. Effects of Reactive Mineral Abundance

[52] To examine the impact of the relative amount of reactive minerals on reaction rate, simulations were con-

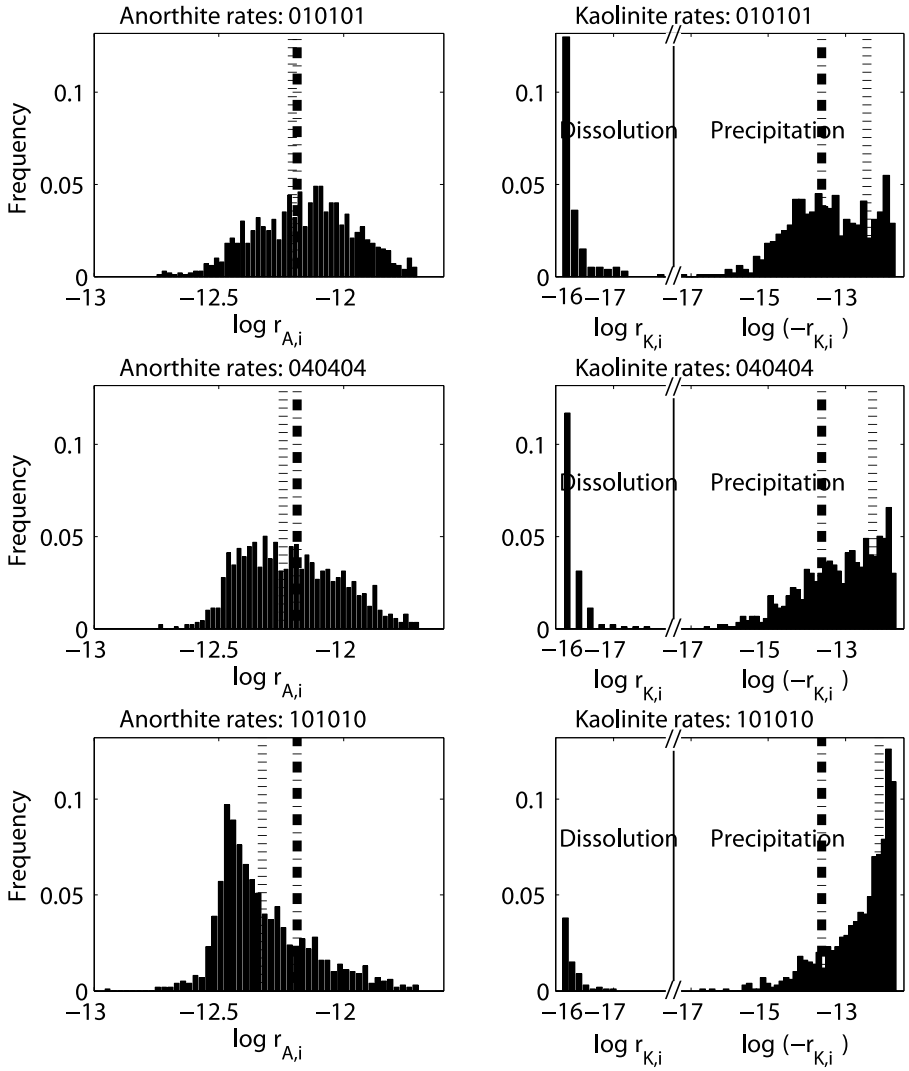

Figure 9. Steady state distributions of the logarithm of reaction rates for reactive clusters of size 010101, 040404, and 101010. The dot-dashed lines are the continuum-scale rates from the continuum model (R_C), and the dotted lines are the continuum-scale rates from the network model (R_N).

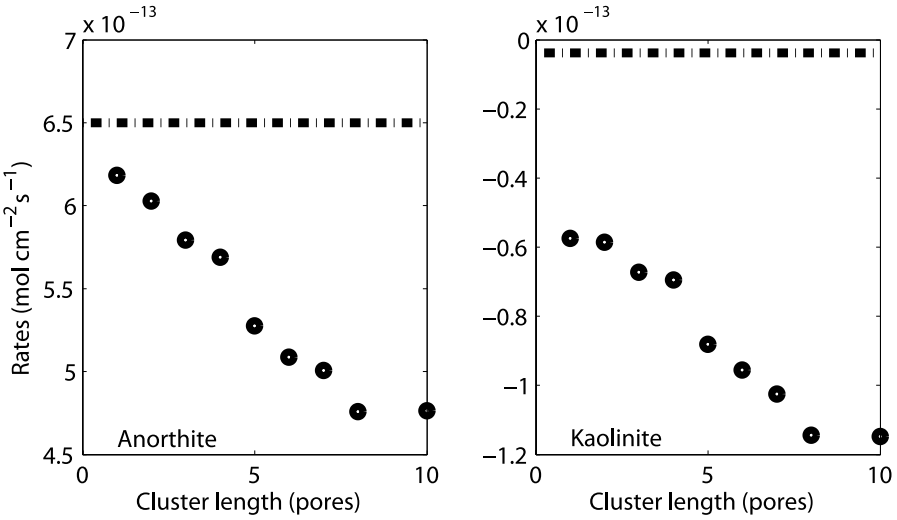

Figure 10. Steady state reaction rates at the continuum scale (R_N) as a function of reactive cluster length. The dot-dashed lines are the rates from the continuum model (R_C).

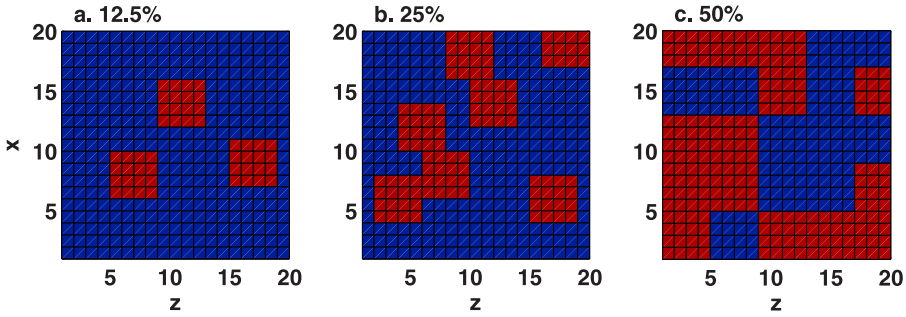

Figure 11. Spatial distributions of reactive minerals in the middle slice of the network ($y = 10$), for the same reactive cluster size 040404 but different percentages of reactive minerals, nominally, 12.5%, 25%, and 50%.

ducted with the percentage of reactive minerals ranging from 6.25% to 50%. For example, Figure 11 shows the spatial distributions of reactive minerals in the middle slice of the network ($y = 10$) for reactive cluster size of 040404, with different percentages of reactive minerals.

[53] At the scale of the entire network, a larger abundance of reactive mineral surface area leads to faster anorthite dissolution rates in units of moles per second. The resulting fast consumption of hydrogen ions leads to a steady state pH that is larger in systems with larger mineral abundance, as is shown in Table 2. As such, the steady state area-normalized anorthite dissolution rate decreases with increasing mineral abundance. For kaolinite, the precipitation rate increases with increasing mineral abundance, because this rate is inversely related to hydrogen ion concentration.

[54] A sample of simulation results from the network model is shown in Table 2 for the case of reactive clusters of size 040404. The variation of pH with increasing mineral abundance that is predicted by the continuum model is slightly larger than the variation in average pH values predicted by the network model. In addition, the minimum and maximum pH values in individual pores are comparable for different abundance of reactive minerals. Since the overall anorthite dissolution rates are dominated by rates in pores with minimum pH values, and the overall kaolinite precipitation rates are dominated by rates in pores with the maximum pH values, the anorthite and kaolinite reaction rates span a much smaller range than those predicted by the continuum model.

[55] Figure 12 shows η values versus reactive cluster length for different percentages of reactive minerals. The largest scaling effects are found with the smallest percentages of reactive minerals. For the 6.25% case, using the continuum model, the anorthite dissolution rate is overestimated by almost a factor of two and the kaolinite precipitation rate is underestimated by more than two orders of magnitude. With a few exceptions, the magnitude of the scaling effect decreases with increasing mineral abundance.

[56] As was explained in section 5.2, η increases with increasing cluster size for anorthite and decreases for kaolinite. However, the extent of change in η is strongly dependent on the amount of reactive mineral. When there is a small amount of reactive mineral present, the change in the scaling effect with reactive cluster size is the largest. When there is a large amount of reactive mineral present, the scaling effects are the smallest and the scaling effects are mostly unaffected by changes in cluster size.

[57] For kaolinite, η is always less than unity, implying that the continuum model always underestimates the precipitation rate for the range of network conditions studied here. For anorthite, both positive and negative η values were observed. For the smallest mineral percentages, 6.25% and 12.5%, the continuum model always overestimated the dissolution rate. For the 50% case, the continuum model always underestimated the dissolution rate. However, for the 25% case, the scaling effect was the smallest and both positive and negative values of η were observed.

6. Discussion

[58] Simulation results have shown that under conditions relevant to CO_2 geological sequestration, mineral spatial distributions can affect reaction rates in porous media, especially when the reactive minerals are present in small amounts, and reactive minerals are distributed in small clusters or clusters oriented transverse to the direction of the main flow. Such effects originate from the differences in the rates of mass transport between reactive and nonreactive pores, depending on the spatial distributions of reactive

Table 2. Steady State Model Simulation Results for Different Percentages of Reactive Mineral Abundance[a]

	Continuum Model			Network Model, Cluster Size 040404		
Reactive Minerals	pH	$R_{C,A}$	$R_{C,K}$	pH	$R_{N,A}$	$R_{N,K}$
6.25%	3.23	8.9×10^{-13}	-3.0×10^{-16}	3.22 (2.97–3.58)	5.9×10^{-13}	-4.9×10^{-14}
12.5%	3.29	6.6×10^{-13}	-4.1×10^{-15}	3.24 (2.95–3.64)	5.4×10^{-13}	-7.1×10^{-14}
25%	3.37	4.7×10^{-13}	-3.2×10^{-14}	3.29 (2.97–3.67)	5.0×10^{-13}	-9.0×10^{-14}
50%	3.44	3.6×10^{-13}	-1.1×10^{-13}	3.35 (2.95–3.75)	4.0×10^{-13}	-1.6×10^{-13}

[a]The pH for the network model is based on volume-averaged concentrations for reactive pores only, and the numbers in the parentheses show the range of pH in reactive pores. All reaction rates are in units of mol cm^{-2} s^{-1}.

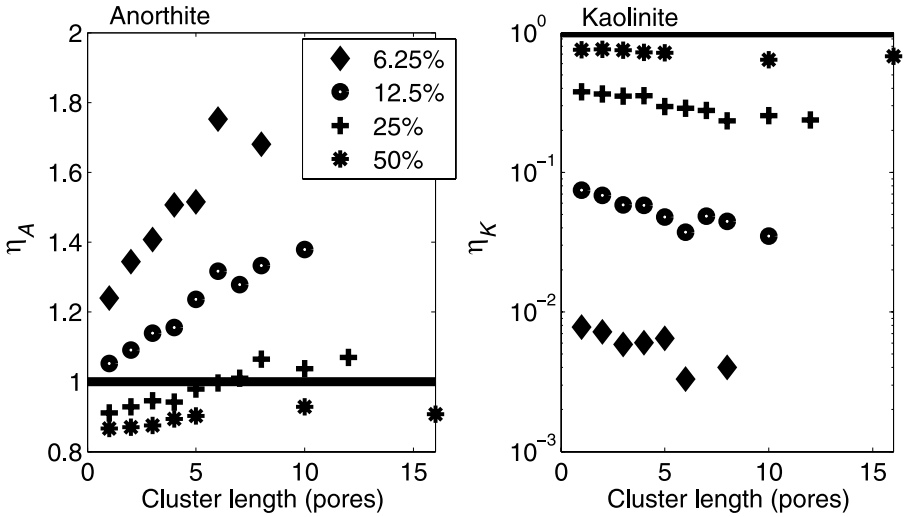

Figure 12. Values of η as a function of reactive cluster size for different percentages of reactive minerals.

minerals. With transverse clusters, the reactive pores adjoin nonreactive pores in the main flow direction; with parallel clusters, they are adjacent mainly in the direction orthogonal to the main flow. Thus, with transverse clusters, there are larger rates of mass transport between reactive and nonreactive pores. Similarly, small clusters enhance mass transport between reactive and nonreactive pores because small clusters lead to a large number of direct connections between reactive and nonreactive pores. For example, with the smallest cluster (010101), each reactive pore is directly connected to as many as six nonreactive pores; with the largest cluster (1000 pores), on average each reactive pore is connected to 0.5 nonreactive pores, an order of magnitude smaller.

[59] Because mass transport is relatively fast with transverse or small clusters, mineral dissolution is also fast under these conditions, due to the constant introduction of unreacted species into reactive pores and the removal of reaction products from reactive pores. As such, large percentages of reactive pores have large anorthite dissolution rates and small kaolinite precipitation rates, which collectively results in large anorthite dissolution rates and small kaolinite precipitation rates at the continuum scale. With parallel or large clusters, the reduced mass transport between reactive and nonreactive pores eventually produces small anorthite dissolution rates and large kaolinite precipitation rates.

[60] With abundant reactive minerals, the effects of mineral spatial distribution are not as significant. Under such conditions, the number of nonreactive pores is relatively small, with many of them surrounded by the reactive pores. As such, the concentrations in nonreactive pores are easily affected by concentrations in reactive pores, and differences in spatial distributions do not make a significant difference in the pore-scale structure of concentrations and reaction rates.

[61] In summary, the scaling effects, i.e., the discrepancies between rates from the network model and those from the continuum model, are larger with large or parallel pore clusters and with small mineral abundance, where the mass transport is not efficient enough to homogenize the concentration field. This reveals the fact that the continuum model, by using spatially averaged properties and representing the entire system as if it is well mixed, does not resolve the pore-scale structure of the system when significant concentration variations develop. As such, it introduces errors in predicting rates using these averaged concentrations. Such scale-dependent reaction rates caused by small-scale concentration variations have been observed be several other studies [*Kapoor et al.*, 1997, 1998; *Meile and Tuncay*, 2006]. *Kapoor et al.* [1997, 1998] found that the small-scale concentration variations, caused by the spatial variations in flow, leads to an overestimation of a bimolecular transformation rate. *Meile and Tuncay* [2006] also observed a difference between the macroscopic rate estimate and the averaged reaction rate at "reaction fronts exhibiting high concentration gradients."

[62] These findings reveal that although at the pore scale (in single pores), the reactions of anorthite and kaolinite are surface-controlled, the chemical heterogeneities of porous media impose conditions under which the continuum-scale reaction rates may be limited by mass transport from pore to pore. The scaling effects may be minimized if advective mass transfer is so slow as to achieve spatially uniform concentrations due to diffusion. On the other hand, if the reaction of interest has a much slower rate (such as quartz), or a less acidic aqueous phase is involved for a pH-dependent reaction, the transport (advection or diffusion) would be fast enough to eliminate small-scale concentration variations so that scaling effects do not develop.

[63] The fact that large scaling effects are found with sparse reactive minerals has interesting implications. In natural porous media, many sedimentary rocks contain small percentages of reactive minerals such as feldspars and clay minerals (in general, the more mature the sedimentary rocks are, the fewer reactive minerals they have). Nonetheless, these small amounts of reactive minerals can affect subsurface water chemistry significantly. In such situations, the mineral spatial distributions can affect the continuum-scale reaction rates significantly, and accurate estimation of reaction rates would require knowledge on the spatial patterns of reactive minerals. In current petrology

and sedimentary geology literature, quantitative information on spatial patterns of reactive minerals is rarely available. This work points to the need for additional research on this topic, as pointed out by previous research on effect of chemical heterogeneities on contaminant transport [*Tompson*, 1993; *Tompson et al.*, 1996; *Espinoza and Valocchi*, 1997, 1998; *Ginn*, 1999].

[64] Although techniques for characterizing pore structure have been advanced, and sophisticated techniques, such as X-ray computed tomography [*Lindquist et al.*, 2000; *Shin et al.*, 2005], have been used in recent years, identification of the pore structure and properties remains the most difficult aspect of network modeling [*Celia et al.*, 1995]. Because of the lack of measurements at the pore scale, this work is based on and limited by a series of simplifying assumptions, including using a regular latticed pore network, and ignoring the spatial correlation of pore volume distribution, correlation between pore coordination number and pore volume, as well as correlation between pore distance and pore volume. Concerning mineral properties, the simplifications include using idealized mineral spatial distribution patterns. These simplifications may affect the magnitude of the reported scaling effects. However, it is our view that the qualitative results, as well as the general principle that fast mass transport eliminates scaling effects, should still hold. These findings suggest that future work that characterizes pore-scale physical and chemical properties is greatly needed [*Peters et al.*, 2006].

[65] Although upscaling only from the scale of tens of micrometers (pore scale) to the scale of several millimeters (''continuum scale''), this study shows the general importance of the scaling effects of chemical reactions in porous media, which has implications for choosing the size of model resolution in reactive transport modeling. If the characteristic scale of chemical heterogeneity is much ''smaller'' than that of a grid block, the system may be considered as a homogeneous system, as with the continuum model; if it is comparable to the size of grid block, ignoring the heterogeneity effects can introduce large errors.

7. Summary and Conclusions

[66] Pore-scale network models that represent sandstones with various spatial distributions of anorthite and kaolinite have been constructed to simulate reactive transport processes, to calculate the corresponding continuum-scale reaction rates, and to examine the impacts of spatial distributions of reactive minerals. The continuum-scale reaction rates from the network models were also compared to the rates from corresponding continuum models that ignore pore-scale heterogeneities. The differences between the rates from the two models were evaluated to measure the scaling effects of reaction kinetics.

[67] Simulation results have shown that with abundant reactive minerals, the scaling effects are minimal and the effects of mineral spatial distributions on effective reaction rates are not significant. With small but typical percentages of reactive minerals, such as 12.5%, there are significant scaling effects so variations in mineral spatial distributions affect the rate of mass transport between reactive and nonreactive pores, the pore-scale distribution of concentrations, as well as the continuum-scale rates. The spatial distributions that reduce the mass transport between reactive and nonreactive pores, such as large reactive clusters and clusters parallel to the flow, result in relatively small anorthite dissolution rates and large kaolinite precipitation rates.

[68] Because the continuum model does not capture the spatial distributions of reactive minerals at the pore scale, it predicts the same continuum-scale reaction rates for various spatial distributions. The scaling effects are largest when small amounts of reactive minerals gather in large clusters or clusters parallel to the main flow direction, which reduces the mass transport between reactive and nonreactive pores. For reactive minerals occupying 12.5% and gathering in one cluster, the anorthite dissolution rates from the two models differ by a factor of 1.4, and kaolinite precipitation rates by a factor of 0.035. The scaling effects increase with reactive cluster size, and with decreasing percentage of reactive minerals. These results provide guidelines for the conditions under which scaling effects are significant in determining mineral reaction rates in porous media.

[69] **Acknowledgments.** This material is based upon work supported by the U.S. Department of Energy under award DE-FG02-05ER15636. The authors also acknowledge BP and Ford Motor Co. for their support of the Carbon Mitigation Initiative at Princeton University. This report was prepared as an account of work sponsored by an agency of the U.S. Government. Neither the U.S. Government nor any agency thereof nor any of their employees make any warranty, express or implied, or assumes any legal liability or responsibility for the accuracy, completeness, or usefulness of any information, apparatus, product, or process disclosed, or represents that its use would not infringe privately owned rights. Reference herein to any specific commercial product, process, or service by trade name, trademark, manufacturer, or otherwise does not necessarily constitute or imply its endorsement, recommendation, or favoring by the U.S. Government or any agency thereof. The views and opinions of authors expressed herein do not necessarily state or reflect those of the United States Government or any agency thereof.

References

Amrhein, C., and D. L. Suarez (1988), The use of a surface complexation model to describe the kinetics of ligand-promoted dissolution of anorthite, *Geochim. Cosmochim. Acta*, *52*(12), 2785–2793.

Berner, R. A., A. C. Lasaga, and R. M. Garrels (1983), The carbonate-silicate geochemical cycle and its effect on atmospheric carbon dioxide over the past 100 million years, *Am. J. Sci.*, *283*, 641–683.

Blatt, H. (1992), *Sedimentary Petrology*, 2nd ed., W. H. Freeman, New York.

Blum, A. E., and L. L. Stillings (1995), Feldspar dissolution kinetics, in *Chemical Weathering Rates of Silicate Minerals*, *Rev. Mineral.*, vol. 31, edited by A. F. White and S. L. Brantley, pp. 291–351, Mineral. Soc. of Am., Washington, D. C.

Blunt, M. J. (2001), Flow in porous media: Pore-network models and multiphase flow, *Curr. Opinion Colloid Interface Sci.*, *6*(3), 197–207.

Bolton, E. W., A. C. Lasaga, and D. M. Rye (1999), Long-term flow/chemistry feedback in a porous medium with heterogenenous permeability: Kinetic control of dissolution and precipitation, *Am. J. Sci.*, *299*, 1–68.

Borgia, G. C., R. J. S. Brown, and P. Fantazzini (1996), Nuclear magnetic resonance relaxivity and surface-to-volume ratio in porous media with a wide distribution of pore sizes, *J. Appl. Phys.*, *79*(7), 3656–3664.

Brady, P. V., and J. V. Walther (1989), Controls on silicate dissolution rates in neutral and basic pH solutions at 25°C, *Geochim. Cosmochim. Acta*, *53*(11), 2823–2830.

Carozzi, A. V. (1993), *Sedimentary Petrography*, Prentice-Hall, Eglewood Cliffs, N. J.

Carroll, S., and K. Knauss (2005), Dependence of labradorite dissolution kinetics on CO_2(aq), al(aq), and temperature, *Chem. Geol.*, *217*(3–4), 213–225.

Carroll, S. A., and J. V. Walther (1990), Kaolinite dissolution at 25°C, 60°C, and 80°C, *Am. J. Sci.*, *290*(7), 797–810.

Celia, M. A., P. C. Reeves, and L. A. Ferrand (1995), Recent advances in pore scale models for multiphase flow in porous-media, *Rev. Geophys.*, *33*, 1049–1057.

Dagan, G. (1990), Transport in heterogeneous porous formations: Spatial moments, ergodicity, and effective dispersion, *Water Resour. Res.*, *26*(6), 1281–1290.

Dagan, G. (2004), On application of stochastic modeling of groundwater flow and transport, *Stochastic Environ. Res. Risk Assess.*, *18*(4), 266–267.

De Windt, L., J. Van Der Lee, and D. Pellegrini (2004), Reactive transport modelling of a spent fuel repository in a stiff clay formation considering excavation damaged zones, *Radiochim. Acta*, *92*(9–11), 841–848.

Dillard, L. A., and M. J. Blunt (2000), Development of a pore network simulation model to study nonaqueous phase liquid dissolution, *Water Resour. Res.*, *36*(2), 439–454.

Duan, Z., and R. Sun (2003), An improved model calculating CO_2 solubility in pure water and aqueous NaCl solutions from 273 to 533 K and from 0 to 2 000 bar, *Chem. Geol.*, *193*(3–4), 257–271.

Dupin, H. J., P. K. Kitanidis, and P. L. McCarty (2001), Pore-scale modeling of biological clogging due to aggregate expansion: A material mechanics approach, *Water Resour. Res.*, *37*(12), 2965–2979.

Espinoza, C., and A. Valocchi (1997), Stochastic analysis of one-dimensional transport of kinetically adsorbing solutes in chemically heterogeneous aquifers, *Water Resour. Res.*, *33*(11), 2429–2445.

Espinoza, C., and A. Valocchi (1998), Temporal moments analysis of transport in chemically heterogeneous porous media, *J. Hydrol. Eng.*, *3*(4), 276–284.

Freeze, R. A. (1975), A stochastic-conceptual analysis of one-dimensional groundwater flow in nonuniform homogeneous media, *Water Resour. Res.*, *11*, 725–741.

Frosch, G. P., J. E. Tillich, R. Haselmeier, M. Holz, and E. Althaus (2000), Probing the pore space of geothermal reservoir sandstones by nuclear magnetic resonance, *Geothermics*, *29*(6), 671–687.

Ganor, J., J. L. Mogollon, and A. C. Lasaga (1995), The effect of pH on kaolinite dissolution rates and on activation-energy, *Geochim. Cosmochim. Acta*, *59*(6), 1037–1052.

Gaus, I., M. Azaroual, and I. Czernichowski-Lauriol (2005), Reactive transport modelling of the impact of CO_2 injection on the clayey cap rock at Sleipner (North Sea), *Chem. Geol.*, *217*(3–4), 319–337.

Gelhar, L. W. (1993), *Stochastic Subsurface Hydrology*, Prentice-Hall, Englewood Cliffs, N. J.

Giammar, D. E., R. G. Bruant, and C. A. Peters (2005), Forsterite dissolution and magnesite precipitation at conditions relevant for deep saline aquifer storage and sequestration of carbon dioxide, *Chem. Geol.*, *217*(3–4), 257–276.

Ginn, T. (1999), On the distribution of multicomponent mixtures over generalized exposure time in subsurface flow and reactive transport: Foundations, and formulations for groundwater age, chemical heterogeneity, and biodegradation, *Water Resour. Res.*, *35*(5), 1395–1407.

Golubev, S., O. Pokrovsky, and J. Schott (2005), Experimental determination of the effect of dissolved CO_2 on the dissolution kinetics of Mg and Ca silicates at 25°C, *Chem. Geol.*, *217*(3–4), 227–238.

Gunter, W. D., E. H. Perkins, and I. Hutcheon (2000), Aquifer disposal of acid gases: Modelling of water-rock reactions for trapping of acid wastes, *Appl. Geochem.*, *15*(8), 1085–1095.

Harter, T. (2003), Basic concepts of groundwater hydrology, *Tech. Rep. Publ. 8083*, Univ. of Calif.

Held, R. J., and M. A. Celia (2001), Pore-scale modeling and upscaling of nonaqueous phase liquid mass transfer, *Water Resour. Res.*, *37*(3), 539–549.

Helgeson, H. C., W. M. Murphy, and P. Aagaard (1984), Thermodynamic and kinetic constraints on reaction-rates among minerals and aqueous-solutions. 2. rate constants, effective surface-area, and the hydrolysis of feldspar, *Geochim. Cosmochim. Acta*, *48*(12), 2405–2432.

Jia, C., K. Shing, and Y. C. Yortsos (1999), Visualization and simulation of non-aqueous phase liquids solubilization in pore networks, *J. Contam. Hydrol.*, *35*(4), 363–387.

Kapoor, V., L. W. Gelhar, and F. Miralles-Wilhelm (1997), Bimolecular second-order reactions in spatially varying flows: Segregation induced scale-dependent transformation rates, *Water Resour. Res.*, *33*(4), 527–536.

Kapoor, V., C. T. Jafvert, and D. A. Lyn (1998), Experimental study of a bimolecular reaction in Poiseuille flow, *Water Resour. Res.*, *34*(8), 1997–2004.

Knapp, R. B. (1989), Spatial and temporal scales of local equilibrium in dynamic fluid-rock systems, *Geochim. Cosmochim. Acta*, *53*, 1955–1964.

Knauss, K., J. Johnson, and C. Steefel (2005), Evaluation of the impact of CO_2, co-contaminant gas, aqueous fluid and reservoir rock interactions on the geologic sequestration of CO_2, *Chem. Geol.*, *217*, 339–350.

Knutson, C. E., C. J. Werth, and A. J. Valocchi (2001), Pore-scale modeling of dissolution from variably distributed nonaqueous phase liquid blobs, *Water Resour. Res.*, *37*(12), 2951–2963.

Kump, L. R., S. L. Brantley, and M. A. Arthur (2000), Chemical weathering, atmospheric CO_2, and climate, *Annu. Rev. Earth Planet. Sci.*, *28*, 611–667.

Lasaga, A. C. (1998), *Kinetic Theory in the Earth Sciences*, Princeton Univ. Press, Princeton, N. J.

Lasaga, A. C., and D. M. Rye (1993), Fluid-flow and chemical-reaction kinetics in metamorphic systems, *Am. J. Sci.*, *293*(5), 361–404.

Le Gallo, Y., O. Bildstein, and E. Brosse (1998), Coupled reaction-flow modeling of diagenetic changes in reservoir permeability, porosity and mineral compositions, *J. Hydrol.*, *209*(1–4), 366–388.

Li, L., C. A. Peters, and M. A. Celia (2006), Upscaling geochemical reaction rates using pore-scale network modeling, *Adv. Water Resour.*, *29*, 1351–1370.

Li, L., C. A. Peters, and M. A. Celia (2007), Reply to ''Comment on upscaling geochemical reaction rates using pore-scale network modeling'' by Peter C. Lichtner and Qinjun Kang, *Adv. Water Resources.*, in press.

Lichtner, P. C. (1985), Continuum model for simultaneous chemical-reactions and mass-transport in hydrothermal systems, *Geochim. Cosmochim. Acta*, *49*(3), 779–800.

Lichtner, P. C. (1996), Continuum formulation of multicomponent-multiphase reactive transport, in *Reactive Transport in Porous Media*, *Rev. Mineral.*, vol. 34, edited by P. C. Lichtner, C. I. Steefel, and E. H. Oelkers, pp. 1–81, Mineral. Soc. of Am., Washington, D. C.

Lichtner, P. C., C. I. Steefel, and E. H. Oelkers (Eds.) (1996), *Reactive Transport in Porous Media*, *Rev. Mineral.*, vol. 34, Mineral. Soc. of Am., Washington, D. C.

Lindquist, W. B., A. Venkatarangan, J. Dunsmuir, and T. F. Wong (2000), Pore and throat size distributions measured from synchrotron X-ray tomographic images of Fontainebleau sandstones, *J. Geophys. Res.*, *105*(B9), 21,509–21,527.

Mayer, A. S., C. T. Kelley, and C. T. Miller (2002), Optimal design for problems involving flow and transport phenomena in saturated subsurface systems, *Adv. Water Resour.*, *25*(8–12), 1233–1256.

Meile, C., and K. Tuncay (2006), Scale dependence of reaction rates in porous media, *Adv. Water Resour.*, *29*(1), 62–71.

Metz, V., B. Kienzler, and W. Schussler (2003), Geochemical evaluation of different groundwater-host rock systems for radioactive waste disposal, *J. Contam. Hydrol.*, *61*(1–4), 265–279.

Morel, F., and J. G. Hering (1993), *Principles and Applications of Aquatic Chemistry*, John Wiley, New York.

Nagy, K. L., A. E. Blum, and A. C. Lasaga (1991), Dissolution and precipitation kinetics of kaolinite at 80° and pH 3: The dependence on solution saturation state, *Am. J. Sci.*, *291*(7), 649–686.

Oelkers, E. (2005), Geochemical aspects of CO_2 sequestration, *Chem. Geol.*, *217*(3–4), 183–186.

Oelkers, E. H., and J. Schott (1995), Experimental study of anorthite dissolution and the relative mechanism of feldspar hydrolysis, *Geochim. Cosmochim. Acta*, *59*(24), 5039–5053.

Oelkers, E., P. Bjørkum, and W. Murphy (1996), A petrographic and computational investigation of quartz cementation and porosity reduction in north sea sandstones, *Am. J. Sci.*, *296*(4), 420–452.

Peters, C. A., J. A. Lewandowski, M. Maier, M. A. Celia, and L. Li (2006), Mineral grain spatial patterns and reaction rate up-scaling, in *Proceedings of the XVI International Conference on Computational Methods in Water Resources*, edited by P. J. Binning et al. (Available at http://proceedings.cmwr-xvi.org/)

Pokrovsky, O., S. Golubev, and J. Schott (2005), Dissolution kinetics of calcite, dolomite and magnesite at 25°C and 0 to 50 atm pCO_2, *Chem. Geol.*, *217*(3–4), 239–255.

Seeboonruang, U., and T. R. Ginn (2006), Upscaling heterogeneity in aquifer reactivity via exposure-time concept: Forward model, *J. Contam. Hydrol.*, *84*(3–4), 127–154.

Sen, P. N., C. Straley, W. Kenyon, and M. S. Wittingham (1990), Surface-to-volume ratio, charge density, nuclear magnetic relaxation, and permeability in clay-bearing sandstones, *Geophysics*, *55*(1), 61–69.

Shin, H., W. B. Lindquist, D. L. Sahagian, and S. R. Song (2005), Analysis of the vesicular structure of basalts, *Comput. Geosci.*, *31*(4), 473–487.

Soler, J., and U. Mader (2005), Interaction between hyperalkaline fluids and rocks hosting repositories for radioactive waste: Reactive transport simulations, *Nucl. Sci. Eng.*, *151*(1), 128–133.

Spycher, N., and K. Pruess (2005), CO_2-H_2O mixtures in the geological sequestration of CO_2. II. Partitioning in chloride brines at 12–100°C and up to 600 bar, *Geochim. Cosmochim. Acta*, *69*(13), 3309–3320.

Steefel, C. I., and A. C. Lasaga (1994), A coupled model for transport of multiple chemical species and kinetic precipitation/dissolution reactions with application to reactive flow in single phase hydrothermal systems, *Am. J. Sci.*, *294*, 529–592.

Steefel, C., and P. Van Cappellen (1990), A new kinetic approach to modeling water-rock interaction: The role of nucleation, precursors, and Ostwald ripening, *Geochim. Cosmochim. Acta*, *54*(10), 2657–2677.

Steefel, C., S. Carroll, P. Zhao, and S. Roberts (2003), Cesium migration in Hanford sediment: A multisite cation exchange model based on laboratory transport experiments, *J. Contam. Hydrol.*, *67*(1–4), 219–246.

Steefel, C. I., D. J. DePaolo, and P. C. Lichtner (2005), Reactive transport modeling: An essential tool and a new research approach for the Earth sciences, *Earth Planet. Sci. Lett.*, *240*, 539–558.

Suchomel, B. J., B. M. Chen, and M. B. Allen (1998), Network model of flow, transport and biofilm effects in porous media, *Transp. Porous Media*, *30*(1), 1–23.

Tompson, A., C. Bruton, W. Bourcier, D. Shumaker, A. Kersting, D. Smith, S. Carle, G. Pawloski, and J. Rard (2000), Simulation of radionuclide migration in groundwater away from an underground nuclear test, in *Mater. Res. Soc. Symp. Proc.*, *608*, 199–210.

Tompson, A. F. B. (1993), Numerical-simulation of chemical migration in physically and chemically heterogeneous porous-media, *Water Resour. Res.*, *29*(11), 3709–3726.

Tompson, A. F. B., and K. J. Jackson (1996), Reactive transport in heterogeneous systems: An overview, in *Reactive Transport in Porous Media*, *Rev. Mineral.*, vol. 34, edited by P. C. Lichtner, C. I. Steefel, and E. H. Oelkers, pp. 269–310, Mineral. Soc. of Am., Washington, D. C.

Tompson, A. F. B., A. L. Schafer, and R. W. Smith (1996), Impacts of physical and chemical heterogeneity on cocontaminant transport in a sandy porous medium, *Water Resour. Res.*, *32*(4), 801–818.

Van der Lee, J., and L. De Windt (2001), Present state and future directions of modeling of geochemistry in hydrogeological systems, *J. Contam. Hydrol.*, *47*(2–4), 265–282.

Walker, J., P. B. Hays, and J. F. Kasting (1981), A negative feedback mechanism for the long-term stabilization of Earth's surface temperatures, *J. Geophys. Res.*, *86*, 9776–9782.

White, A. F., and S. L. Brantley (1995), Chemical weathering rates of silicate minerals: An overview, in *Chemical Weathering Rates of Silicate Minerals*, *Rev. Mineral.*, vol. 31, edited by A. F. White and S. L. Brantley, pp. 1–22, Mineral. Soc. of Am., Washington, D. C.

White, S., R. Allis, T. Chidsey, C. Morgan, W. Gwynn, J. Moore, and M. Adams (2005), Simulation of reactive transport of injected CO_2 on the Colorado Plateau, Utah, USA, *Chem. Geol.*, *217*(3–4), 387–405.

Xu, T., J. Apps, and K. Pruess (2004), Numerical simulation of CO_2 disposal by mineral trapping in deep aquifers, *Appl. Geochem.*, *19*(6), 917–936.

Xu, T., J. A. Apps, and K. Pruess (2003), Reactive geochemical transport simulation to study mineral trapping for CO_2 disposal in deep arenaceous formations, *J. Geophys. Res.*, *108*(B2), 2071, doi:10.1029/2002JB001979.

Xu, T. F., S. P. White, K. Pruess, and G. H. Brimhall (2000), Modeling of pyrite oxidation in saturated and unsaturated subsurface flow systems, *Transp. Porous Media*, *39*(1), 25–56.

Zhou, D. G., L. A. Dillard, and M. J. Blunt (2000), A physically based model of dissolution of nonaqueous phase liquids in the saturated zone, *Transp. Porous Media*, *39*(2), 227–255.

M. A. Celia and C. A. Peters, Department of Civil and Environmental Engineering, Princeton University, Princeton, NJ 08544, USA. (celia@princeton.edu; cap@princeton.edu)

L. Li, Earth Sciences Division, Lawrence Berkeley National Laboratory, 1 Cyclotron Road, MS 90-1116, Berkeley, CA 94720, USA. (lili@lbl.gov)